Hydrodynamic self-focusing in a parallel microfluidic device through cross-filtration

S. Torino,[1,2,a)] M. Iodice,[1] I. Rendina,[1] G. Coppola,[1] and E. Schonbrun[2]
[1]*Institute for Microelectronics and Microsystems, National Research Council, Naples, Italy*
[2]*Rowland Institute at Harvard, Harvard University, 100 E. Land Blvd., Cambridge, Massachusetts 02142, USA*

(Received 1 September 2015; accepted 10 November 2015; published online 20 November 2015)

The flow focusing is a fundamental prior step in order to sort, analyze, and detect particles or cells. The standard hydrodynamic approach requires two fluids to be injected into the microfluidic device: one containing the sample and the other one, called the sheath fluid, allows squeezing the sample fluid into a narrow stream. The major drawback of this approach is the high complexity of the layout for microfluidic devices when parallel streams are required. In this work, we present a novel parallelized microfluidic device that enables hydrodynamic focusing in each microchannel using a single feed flow. At each of the parallel channels, a cross-filter region is present that allows removing fluid from the sample fluid. This fluid is used to create local sheath fluids that hydrodynamically pinch the sample fluid. The great advantage of the proposed device is that, since only one inlet is needed, multiple parallel micro-channels can be easily introduced into the design. In the paper, the design method is described and the numerical simulations performed to define the optimal design are summarized. Moreover, the operational functionality of devices tested by using both polystyrene beads and Acute Lymphoid Leukemia cells are shown.
[http://dx.doi.org/10.1063/1.4936260]

I. INTRODUCTION

In the past few years, microfluidic devices have shown great promise in numerous research fields. In fact, this technological platform allows obtaining significant results on over expanding fields, going from medicine[1,2] to biology, and from environmental monitoring[3] to aerospace applications.[4] The development of more complex and effective microfluidic devices strictly depends on the possibility to address challenging needs, such as miniaturized and light devices, low consumption of samples and reagents, complex sample preparation, short time-to-result, and simple readout. Recent developments in microfluidic technology offer good solutions to help in managing the complexity of the future lab-on-chip devices allowing the miniaturization, integration, automation, and parallelization of many bio-chemical processes. Several reviews have been published in different fields of applications to demonstrate the versatility and efficiency of the microfluidic approach.[5–7]

In many of these devices, the focusing of particles into a tight stream is a fundamental prior step in order to sort, analyze, and detect them.

Moreover, the focusing of particles to the centre of a micro-channel also prevents them from the influence of the microchannel walls (such as cell adsorption, light scattering). Since microfluidic technology has been introduced, various methods have been exploited to achieve particle/cell focusing. In particular, the focusing can be obtained by either the application of an external force[8–20] or appropriate-shaped microchannels.[21–26] This latter passive method, unlike the first one, requires easier and cheaper fabrication processes and avoids the

[a)]Author to whom correspondence should be addressed. Electronic mail: stefania.torino@na.imm.cnr.it

requirement of sophisticated external set-ups. Different approaches have been recently proposed to induce a passive particle/cell focusing: for instance, hydrodynamic focusing, which uses at least two sheath flows to confine the particles;[27–30] hydrophoretic drifting, which allows one to focus particles by exploiting the pressure field induced by mechanical obstacles placed into the channel;[31,32] and inertial focusing, which uses the inertia of the fluids around the particles to force them into a confined stream.[33–36] These last two approaches can offer an efficient focusing, even if some limitations have to be taken into account. For example, particle/cell size dependence and limited throughput are the main disadvantages of the hydrophoretic approach, whereas a complex design and long channels are the principal limitations for the inertial approach. Besides these approaches, several other methods for particle/cell focusing based on hydrodynamic mechanisms have been adopted,[37] such as viscoelastic focusing,[38] in which the target objects are aligned by using a non-Newtonian fluid as buffer solution; or focusing based on the Dean Flow[39] that is generated in a curved channel in the presence of inertial flows. Some problems and limitations introduced by the afore-listed approaches can be avoided in microfluidic devices based on hydrodynamic focusing. Even if the hydro-focusing method requires a complex and unwieldy management of the sheath fluids, one way to employ a lower number of additional flows is to reduce the dimensionality of the focusing, utilizing devices that achieve a two-dimensional focusing rather than a 3D focusing. In this case, the alignment along the third dimension is achieved realizing a microchannel with a height comparable to the particle size. However, with this geometrical configuration, the flow rate has to be set at a low level in order to reduce the clogging probability. As a consequence, fewer cells will pass through the channel in a same temporal window, by bringing also to an undesired reduction of the system throughput. To address these restrictions, a possible solution is the parallelization, which is one of the main advantages introduced by microfluidic technology. Indeed, having more channels working simultaneously allows reducing the total fluid velocity, but at the same time, the overall throughput of the device is not drastically reduced. Moreover, the parallelization approach allows the developing, in a microfluidic regime, of the "imaging flow cytometry." In fact, even if flow cytometry is the gold-standard technique used for blood/cell analysis, there is a high interest among the medical community on the combination of the quantitative information obtained from the collection of the fluorescence signals with the imaging of the cells under analysis.[40,41] Thus, the possibility to exploit parallel multiple channels working simultaneously with shared inputs has recently been demonstrated.[34,42–45] In this scientific context, using the sheath-flow based parallelized system is not possible using a single layer microfluidic device. In this paper, we propose a new method, named self-hydrodynamic focusing, which allows achieving a sheath flow focusing using only one inlet for the sample fluid. In particular, a crossflow filtration has been adopted to separate the required sheath fluids from the feed fluid. The cross-filter is realized through two micropillar arrays,[46–48] where the distance between two consecutive micropillars is chosen depending on the size of the particle/cell to focus. In this way, only the fluid can cross the pillar-type filter, while particles/cells under investigation are forced to stay in the centre region. After the filtration region, the "sample flow," from the centre region, is pinched between the two self-generated "sheath streams" coming from the lateral channels. The micropillars arrays are positioned in order to allow a feed fluid to travel obliquely across the filter surface, rather than in a dead-end configuration. The principal advantage of this placement is that the pillar-type filter is continuously washed during the filtration process, reducing the clogging probability and so increasing the operation time of the microfluidic device.[49–52] A focusing based on the particles filtration has previously been proposed.[53–56] In particular, Yamada *et al.*[53] have used the "hydrodynamic filtration" to focus microparticles. The operational principle consists of separating part of the buffer solution from the sample fluid by introducing lateral channels that orthogonally intersect the central one. The design allows avoiding particles bigger than a certain size to move into the lateral channels. Then, the buffer solution is recombined with the sample fluid into the main central channel, and as a result, hydrodynamic focusing is achieved. In this device, the design phase has to be focused on choosing the right ratio between the width of the central and lateral channels in order to force cells or particles to not follow the fluid stream that moves laterally. On the other hand, Austin's

Group[55,56] has exploited the deterministic lateral displacement (DLD) for particle focusing. In particular, several arrays of pillars, with each row shifted with respect to the previous one, are adopted. The fluid passing through the pillars follows certain streamlines and different pathways are set up. According to their size, particles will follow one of the defined pathways. The authors have demonstrated that by means of their approach it is possible to focus particles of different sizes in different streams. The focusing principle is based on a precise design of the matrix of pillars, since the right position of the pillars into the matrix determines the correct operation of the device. However, for both the approaches, either the presence of the lateral channels[53] or the microstructured post arrays[55] makes complex and/or cumbersome the extension of operating principles into parallelized microfluidic devices. In our approach, a single line of pillars has been used in order to keep the size limited. Even in our approach, the size of the filtering region and, in particular, the distance between two consecutive pillars depend on the target application. The pillar's gap size will determine the cut-off size of the cells that can be focused, since cells or particles that are smaller will be able to cross the filter membrane. Once the size of both the pillar and the gap is defined according to the particle/cell under test, the width of the focused stream, and therefore the sheath-to-sample flow ratio, is mainly a function of three geometrical parameters: the length of the filter region (L_f), the width of the lateral channels (W_L), and the inclination angle of the pillar arrays (φ). This dependence has been studied, and the results have been used to fabricate three types of microfluidic devices. These devices were characterized using polystyrene beads with different diameters.

Finally, self-hydrodynamic focusing was demonstrated with B-cell Acute Lymphoid Leukemia (B-ALL) cells. B-ALL is a clonal malignant disease that originates in a single cell and is characterized by an accumulation of blast B-cells resulting in the suppression of normal hematopoiesis and infiltration of various extra-medullary sites. B-cells proliferate uncontrollably and are found in large numbers in the peripheral blood. For this reason, it is interesting to detect, count, and, at the same time, observe them, within the analysis of a patient blood sample. The abnormal cells are arrested in the lymphoblast stage of the normal maturation pathway.[57] ALL is one of the four main categories of human leukemia and the majority of ALLs are of the B-cell type.[58] In our experiment, we used B-cell precursor lymphoblastic cells from the MN 60 cell line that are an average size of 5–8 μm. A combination of cytometric and imaging analysis of these cells could be really useful for medical scientist and biologists.

II. PRINCIPLE AND THEORETICAL BACKGROUD

An overview of the developed microfluidic device is shown in Fig. 1(a). The feed flow containing particles comes from only one inlet, and then it is split into eight parallel microchannels. At each one of the parallel channels, a self-focusing region is introduced: it consists of two micro-pillars arrays, where the gaps between the pillars operate as pores of a filter

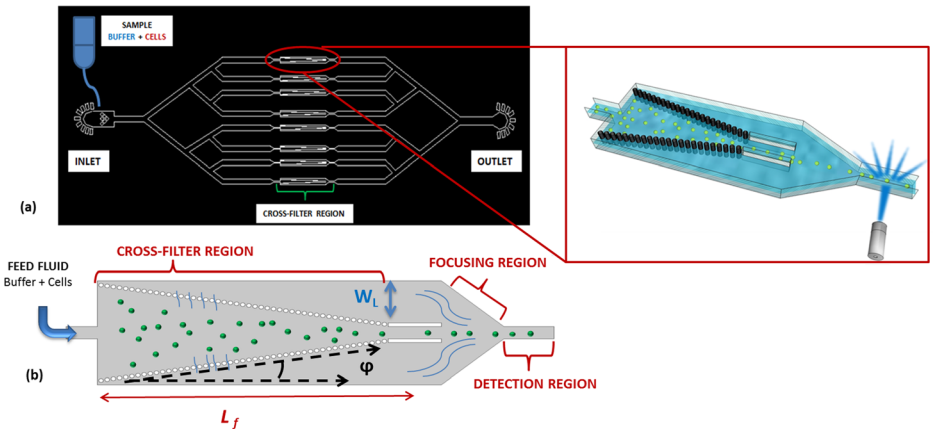

FIG. 1. (a) CAD design of the parallelized microfluidic device. (b) Operating principle of the cross filter region.

membrane (Fig. 1(b)). The micropillar arrays are positioned to recreate a crossfilter configuration,[45,46] where the fluid flows parallel to the filter pores, in contrast to what happens in a traditional dead-end filter[47] in which the fluid direction is perpendicular to the filter surface. By means of this configuration, the micro-pillar arrays are substantially washed away during the filtration process. Therefore, a design in which both the filter length and the pillar position are optimized will reduce the clogging probability. The gap size between the micro-pillars is chosen according to the target particle/cell size. In particular, this gap must be smaller than the mean particle diameter. In this way, when the feed fluid comes into the filtration region, particles whose diameters are larger than the gap never go through the lateral channels, whereas the buffer solution (i.e., filtrate fluid) passes through the micropillar arrays. At the so-called focusing region, a standard sheath-based focusing configuration is obtained. Indeed, the self-generated sheath fluid, coming from the lateral channels, and the sample fluid, coming from the centre region, are recombined. Geometrical design of both the crossflow filter and the lateral channels allows controlling the sheath-to-sample flow ratio and thus the width of the focused stream.

A. The self-focusing region

The self-focusing region configuration determines the flow rate both in the central channel and in lateral ones. The two micropillar arrays are symmetrically positioned with respect to the horizontal centreline so the flow rates (Q_{sh}) inside the two lateral channels are equal. From Hagen–Poiseuille's equation,[59] the pressure drop (ΔP) in a non-compressive Newtonian fluid in laminar flow is related to the flow rate Q through the hydrodynamic resistance of the microchannel (R_h), i.e.,

$$Q = \frac{\Delta P}{R_h}.$$

For an arbitrary cross-sectional shape of the microchannel, R_h[59] is

$$R_h = \gamma \frac{2\mu L p^2}{A^3},$$

where L is the length of the channel, μ is the viscosity of the liquid, p is the perimeter and A the area of the channel cross-section, and γ is a dimensionless factor depending on the channel geometry. Each pore of the pillar-type filter acts as a microchannel with its hydrodynamic resistance.

Thus, the flow rate through the i-th pore (ΔQ_i) depends on both the hydrodynamic resistance of that element and the corresponding pressure drop across that element (ΔP_i). In particular, fixing the pillar shape, ΔQ_i is mainly a function of two parameters

$$\Delta Q_i \propto f(\Delta P_i, s),$$

where s is the gap size to choose according to the target particle/cell size. The whole crossfilter can be represented as a series of independent pores (Fig. 2), so, at the lateral channels, the total self-generated sheath flow rate is given by

$$Q_{sh} = \sum_{i}^{N} \Delta Q_i$$

with N the total number of pores in the micropillars array.

If Q_0 is the incoming flow rate, the sheath to sample flow ratio r that determines the diameter d of the focused stream is

$$r = \frac{Q_{sh}}{Q_{sa}} = \frac{Q_{sh}}{Q_0 - 2Q_{sh}} = \frac{1}{\frac{Q_0}{Q_{sh}} - 2}.$$

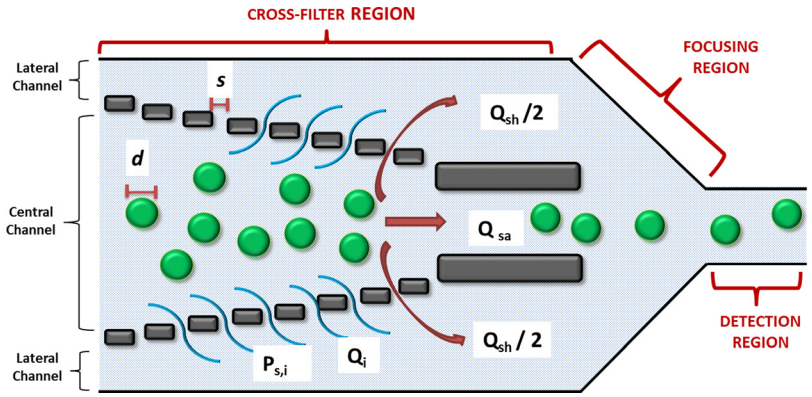

FIG. 2. Schematic of the cross-filter separation region. The gap/pore size (s) has to be chosen in order to be smaller than the target particles/cells diameter ($s < d$). The volume of fluid crossing the filter barrier and moving to the lateral channels at each i-th pore (Q_i) determines the total sheath flow rate (Q_{sh}). The fluid containing the particles/cells, confined at the central channel will act as sample fluid.

Thus, d just depends upon the filter geometrical parameters that determine the self-generated fluids, i.e., the length of the filter region L_f, the width of the lateral channels W_L, and the inclination angle of the pillar arrays φ.

The inclination of the pillar arrays plays a significant role in controlling the pressure drop across the filter region. We studied by means of fluid dynamics simulations the pressure profile along the filter region for a configuration with $\varphi = 0°$ and for one with $\varphi = 1.5°$. Figs. 3(a) and 3(b) show the pressure profile at the central and lateral channels, for the configuration with straight and inclined posts, respectively. In the first case, the pressure in the central channel becomes lower than the pressure in the lateral channel after a length of about 2 mm. On the other hand, for an inclined configuration, the pressure in the central channel is higher than the pressure in the lateral one for all the filter lengths. This means that the difference $\Delta P_i = (P_{c,i} - P_{s,i})$ is always positive. The same results are visualized in Fig. 3(c), where the inversion of the flowing direction due to the absent pillar arrays inclination is highlighted.

III. MATERIALS AND METHODS

A. Device design

By means of parametric numerical simulations performed using the COMSOL Multiphysics (Comsol, Inc., MA, USA) live-link for Matlab (The MathWorks, Inc., MA, USA), different cross-filter geometries were studied. For each of them, the sheath-to-sample flow ratio $r = Q_{sh}/Q_{sa}$ was evaluated. The ratio r indicates how much the sheath fluid is able to confine the sample fluid at the end of the filter region and, therefore, it also determines the width of the focused stream. So, according to the mean diameter of the target cells, by meaning of numerical simulations, we were able to predict which values of the three critical geometrical parameters have to be chosen in order to achieve the desired value of r. The complete analysis has been performed by combining different values of these geometrical parameters and allowed us to obtain the expected value of r for each filter geometry. From the results, we were able to build design-charts useful to find the right device for a desired target cell size. These design charts report all the possible combinations of the geometrical parameters that allow obtaining a specific value of the ratio r. To build these charts, the gap s between the pillar was set to 5 μm in order to allow the focusing of particles and/or cells with a dimension around 10 μm. Moreover, the thickness of the channels was set at 10 μm, whereas the width of the channels downstream of the self-focusing region (i.e., the channel of the detection region) was 50 μm. The width of the lateral channels (W_L) varied from 50 to 250 μm; the length of the filter region (L_f) ranged from 0 to 2500 μm; the inclination angle of the pillar arrays (φ) was in the range [0°–30°]. In Fig. 4, an example of two generated design charts is reported.

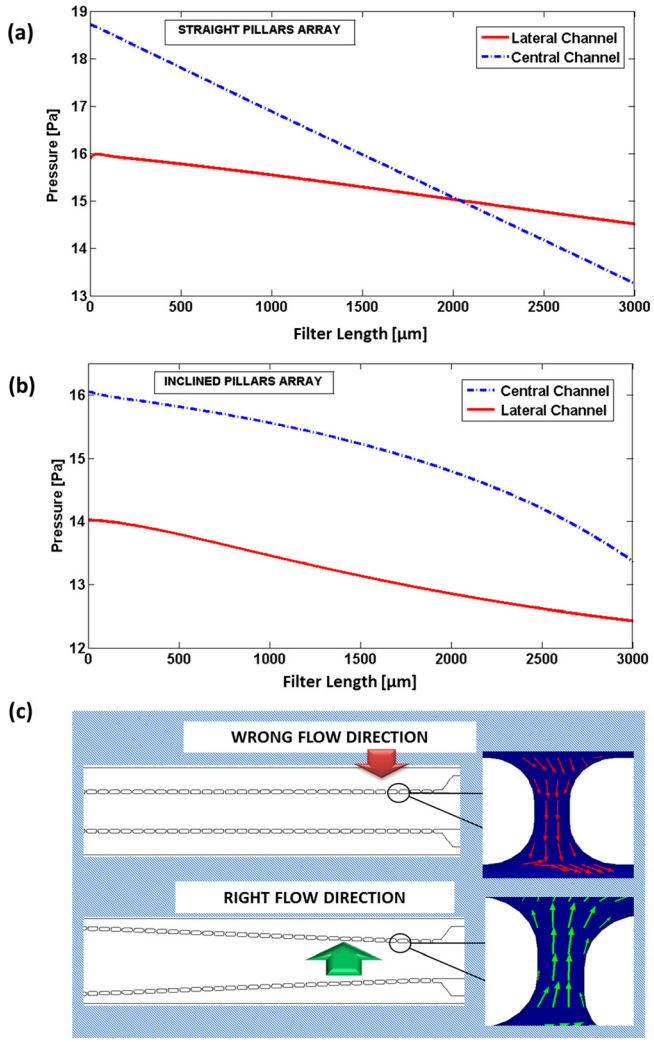

FIG. 3. (a) Pressure profile at the central and lateral channel for a configuration with the pillars array slightly inclined. (b) Pressure profile at the central and lateral channel for a configuration with the pillars array without any inclination. (c) Inversion of the flow direction for a configuration with $\varphi = 0°$ (up in the image). The effect is avoided by adding a slight inclination $\varphi = 1.5°$ (down in the image).

In each plot, the sheath-to-sample flow ratio is a function of the length of the filter region and the width of the lateral channels. Each one of the two charts refers to different values of the inclination angle of the pillar arrays.

On the other hand, the relationship between the diameter d of the focused stream in the interrogation region and the ratio r is illustrated in Fig. 5. Thus, according to the stream diameter d required to confine the target particles/cells, Fig. 5 allows evaluating the corresponding sheath-to-sample flow ratio. A different set of the three geometrical parameters can be selected from the design chart to obtain the required sheath-to-sample flow ratio. It is worth noting that larger inclination angles enable more compact devices, but a higher probability of clogging.

Three different microfluidic devices were realized to confined particles with a diameter of 10 μm. In particular, each device was designed to confine the particles into a stream with a different diameter: weak focusing ($d > 20\,\mu$m), medium focusing ($d \approx 15\,\mu$m), and strong confinement ($d \approx 10\,\mu$m). In order to achieve these stream diameters, the required flow ratio r can be estimated from Fig. 5; in particular, $r < 1$ for the weak focusing, $r \approx 2.5$ for the medium focusing, and $r \approx 6$ for the strong focusing. The geometrical parameters of the three different devices were chosen from the design charts reported in Fig. 4. These parameters are summarized in

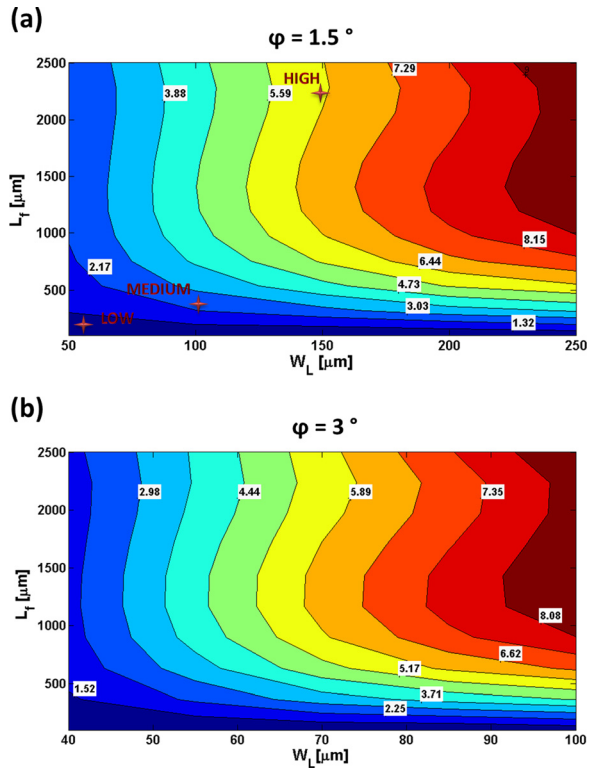

FIG. 4. COMSOL—MATLAB simulation results. In each one of the two design charts, the sheath-to-sample flow ratio (r) is a function of the length of the filter region, and the width of the lateral channel. Each map is parameterized for a value of the inclination angle of the pillar arrays φ of 1.5° (a) and 3° (b). The color scale bar goes from blue, for the lowest values of r, to red for the highest values of r. In (a), the stars refer to the parameters chosen for the three realized devices, also reported in Table I.

Table I. In Fig. 6, the Poincaré maps simulated for the medium and strong focusing device are shown. In particular, the particle positions, for a cut plane at the detection region, confirm the accuracy of the design procedure.

B. Clogging evaluation

In our devices, the crossflow filtration has been adopted to self-generate the required sheath fluids useful for the particle/cell focusing. As well as in any filtration process, the clogging of

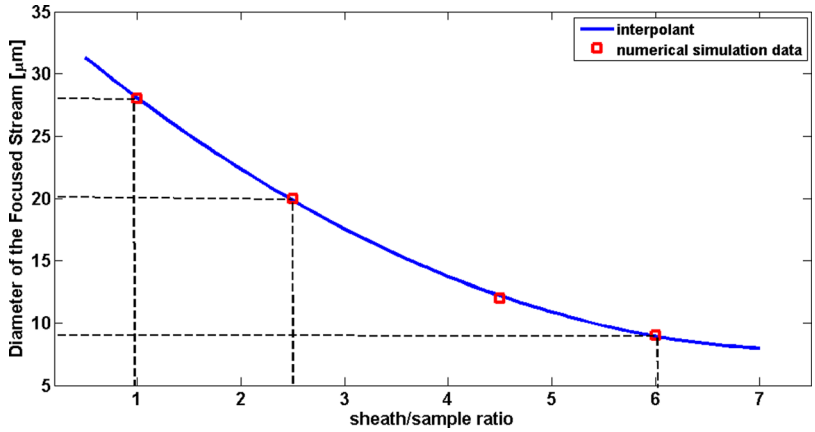

FIG. 5. The graph shows the relationship between the diameter of the focused stream and the sheath to sample ratio in the designed devices.

TABLE I. The geometrical parameters of the cross-filter region for the three realized devices sheath/sample ratio r, length of the filter region L, the width of the lateral channels W_L, the inclination of the pillars arrays φ, and the number of the pillars arrays.

Focusing	d (μm)	r	L_f (μm)	W_L (μm)	φ (°)	N
Weak	>20	<1	100	55	1.5	5
Medium	15	≈2.5	450	100	1.5	22
Strong	10	≈6	2400	140	1.5	120

the membrane is the main issue to overcome. In our devices, the inclination angle of the pillar arrays was chosen in order to allow a continuum washing of the filter and thus to reduce the clogging probability. In particular, we decided to guarantee an operation time of the microfluidic devices of about 1 h that should be adequate for the majority of the devices for cytometric analysis. This point is critical in defining the optimal filter configuration. Indeed, as it can be deduced from the design charts, there are multiple combinations of the three critical parameters that allow achieving a desired sheath-sample flow ratio, and therefore a required diameter of the focused stream. For this reason, considering the desired operation time for the device, we have been able to select the more suitable geometries. In particular, the performed experiments have highlighted that in order to ensure an operation time of at least 1 h, even for low flow rate (50 μl/min), the pillar arrays have to be slightly inclined, and at the same time, a longer cross-filter region is required. In this way, (1) the low inclination limits the tendency of particles/cells in moving through the filter; (2) the higher length of the filter region will correspond to a higher number of pillars, and therefore of filter pores. This latter point gives a significant contribution in limiting the filter clogging and increasing the operation time of the device. Taking into consideration these theoretical assumptions, and considering experimental preliminary tests, we decided to adopt for our devices an inclination of the pillar array of 1.5°.

C. Device fabrication

In order to prove the aforedescribed self-focusing approach, different microfluidic chips with 8 parallel straight channels were realized using the standard PDMS (polydimethylsiloxane) soft-lithography technique. A Silicon master mold was patterned using a photolithography process. In particular, a silicon wafer was cleaned by sonication in acetone and isopropyl alcohol for 10 min each, and blown dry with nitrogen. The cleaned wafer was spin-coated with a negative photoresist (SU8–3010, MicroChem Corp., MA, USA) at 3000 rpm for 30 s to obtain a thickness of 11 μm. This layer was exposed to UV-light through a designed Cr-photomask, developed (SU8 developer, MicroChem Corp., MA, USA) for about 10 min and washed in isopropyl alcohol.

80 g of PDMS oligomer and hardener (10:1 w/w) mixture were poured onto the Silicon mold and degassed for 30 min to remove all trapped bubbles. The degassed mold was then

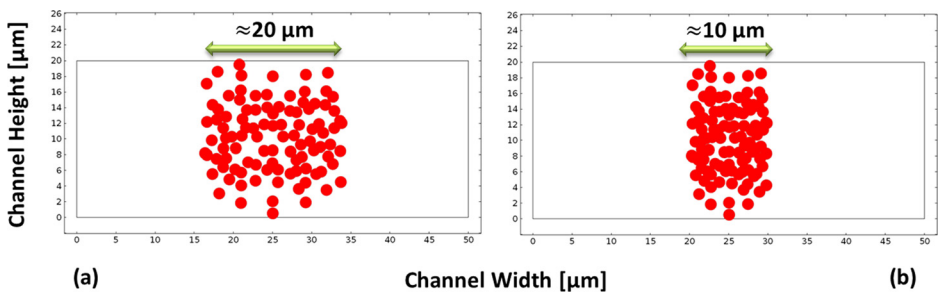

FIG. 6. The Poincaré maps show the expected diameter of the focused stream for the medium (a) and the strong (b) focusing device configuration. Notice that in the plot the particles size is not in scale.

cured on a levelled out plate at 80 °C for 1 h. The cured PDMS was gently peeled from the master and punched for tubing inputs/outputs paying attention to avoid the possible collapse of the PDMS pillars. The PDMS cast and glass slides were exposed to an oxygen plasma (Oxford Instruments, PlasmaLab80+) for 10 s and then immediately placed in contact to irreversibly seal the microfluidic devices. Microfluidic channels were washed with isopropyl alcohol and used after 1 day in order to be sure that the PDMS surface returns to pre-plasma state preventing the adhesion of particles and/or cells. Optical images of a realized microfluidic device are illustrated in Fig. 7.

D. Sample preparation

Experimental results were performed using either polystyrene beads with different diameters and B-cell precursor lymphoblastic cells from the MN 60 cell line. In particular, both isolated and mixed polystyrene particles (Duke Scientific Corporation) were employed to fully characterize the realized devices. Polystyrene beads were suspended in a mixture of PBS (Phosphate Buffer Saline) and BSA (Bovine Serum Albumine) solution to reach a final particle concentration of 5×10^6 beads/ml. A total of 300 μl of feed fluid was prepared by using B-cell precursor lymphoblastic cells from the MN 60 cell line (5–8 μm). 150 μl of MN60 cells in solution were added to 150 μl of blue food dye. In this way, the contrast between cells and the background is increased.

Moreover, for the experiment related to the particle counting, 150 μl of 7.5 μm diameter polystyrene particles (Bags Labs) were mixed to 800 μl of PBS (Phosphate Buffered Saline), obtaining a final concentration of about 400 particles/μl.

E. Experimental set-up

The self-induced hydrodynamic focusing was performed using either particle or cell suspensions for the feed flow from the inlet port. A syringe pump was used to drive the feed flow through the device. Images of the focusing effect in one of the eight parallel channels were acquired using an objective microscope (20×) coupled with CMOS camera (Teledyne DALSA, Inc.,) that allows an acquisition rate up to 1000 fps. A red Light Emitting Diode (LED) was used to illuminate the microfluidic devices. In order to allow a precise alignment of the whole system, both the microfluidic device and the output objective microscope were positioned on micrometer positioning stages.

IV. RESULTS AND DISCUSSIONS

The self-focusing approach was tested on different microfluidic chip families with 8 parallel straight channels. In particular, each device family is relative to different focusing diameters. In order to experimentally evaluate the sheath-to-sample flow ratio, a Particle Image Velocimetry

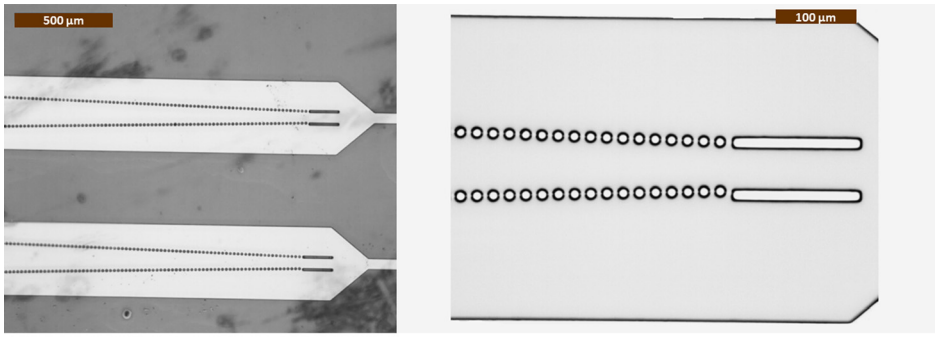

FIG. 7. (a) Images of two of the eight crossflow filtration regions for realized devices with $r \approx 6$. (b) Detail of the micropillar arrays.

(PIV)[60,61] analysis was performed. In particular, in order to calculate speed and direction of the flows inside the focusing region, a feed fluid with a mix of 2 μm and 10 μm polystyrene beads was pumped through the microchannels. 20 videos, each of them with 1500 frames, were acquired.

By means of a Matlab image processing, we were able to discriminate the position for the 2 μm and 10 μm beads. In Fig. 8(a), the bead distribution obtained for the device that induces the weaker focusing diameter ($d > 20\,\mu$m, $r < 1$) is reported. As we expected, the smallest beads were distributed all over the channel, whilst the bigger ones were confined at the central channel (Fig. 8(a)). The velocity map at the end of the filter region, where the self-produced sheath and the sample fluids recombine, is illustrated in Fig. 8(b). Averaging the velocity matrixes obtained from the 20 videos along the line illustrated in Fig. 8(b), the final velocity profile can be achieved (Fig. 8(c)).

From this profile, a sheath to sample ratio of about 1 was estimated in agreement with the numerical simulations. The same approach was applied to the other families of microfluidic devices confirming the simulation data.

As we have reported above in this paper, the main advantage of the proposed approach is the possibility to combine hydrodynamic focusing with a parallelized system. Fig. 9 shows cells flowing in two channels imaged at the same time. We used a traditional imaging set-up for acquiring the data, so we needed at least a 10× objective in order that 10 μm cells or particles could be visible. Specific imaging techniques[45] can be adopted in order to allow imaging of flowing objects in all eight parallel channels.

Each family of microfluidic devices was also tested with the MN 60 cells. The effect of the self-induced hydrodynamic focusing on the MN 60 cells for the strong focusing device ($d \approx 10\,\mu$m, $r = 6$) is reported in movie 1 in the supplementary material.[65] In particular, in Fig. 10(a), the positions of the MN 60 cells inside the detection region are shown, whereas in Fig. 10(b), a magnification of the detection area for the same image is reported. The red dots refer

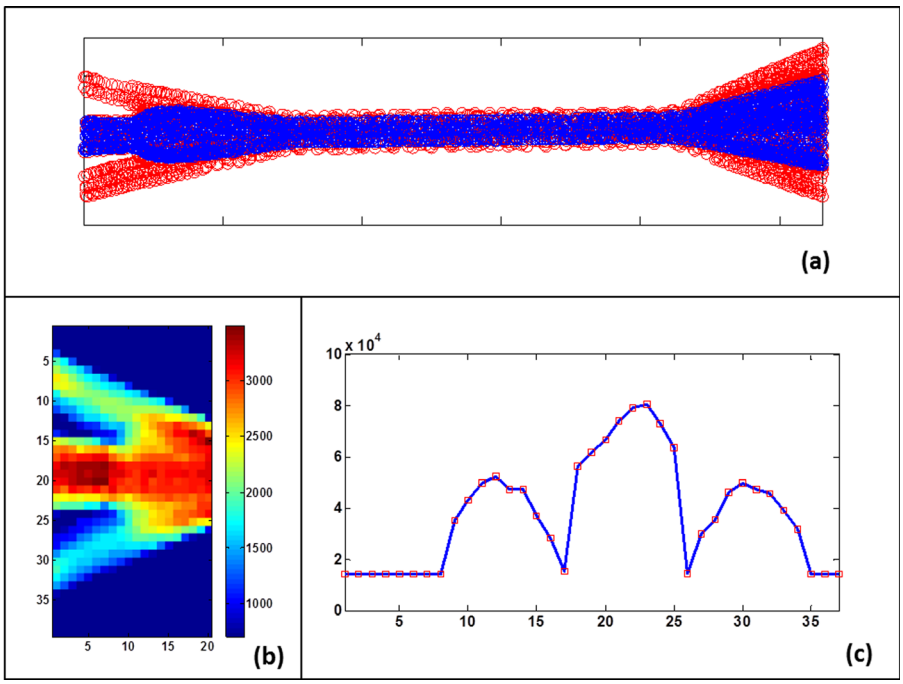

FIG. 8. (a) Matlab Image processing analysis. Position of the particles centroids. The 2 μm particles (RED) can move laterally though the filter, whilst the 10 μm ones (BLUE) stay confined at the centre. (b) Velocity Map obtained by the Particle Image Velocimetry (PIV) analysis. The velocity values are in μm/s. (c) Velocity Profile at the end of the filter region, obtained from the PIV velocity map. The profile allows one to have an estimation of the sheath to sample ratio r for the tested device. For this case, $r \approx 1$, value in agreement with what is expected from the numerical simulations.

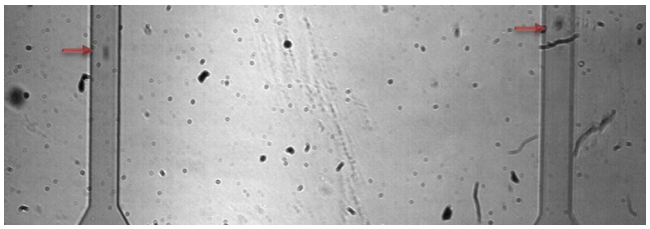

FIG. 9. The figure shows how with a parallelized microfluidic device it is possible to image cells flowing in two channels at the same time. With a traditional imaging set-up, in order to see 10 μm cells or particles, we need at least a 10× objective. This limits the area that can be imaged. By the means of a different imaging technique,[45] it could be possible to have images of cells flowing in all eight channels.

to the cell centroid's positions. It can be seen that cells stay confined in a range of about 4 pixels that correspond to about 10 μm. From the image, it is clear that the stream is not exactly focused at the centre, but it slightly shifted on the left side. This effect reflects the asymmetry present in the CAD design used for making the photolithographic mask.

Moreover, the analysis of the cells' distribution showed that for the device with $r = 6$, 90% of the total cells (351/391 counts) stay confined within the focused stream of 10 μm (Fig. 11(a)), against a channel width of 50 μm.

On the contrary, for the medium configuration ($r = 2.5$), only 57% of the total cells (207/347) stayed confined in the 10 μm focused stream (Fig. 11(b)), whilst for this device, the percentage of cells confined in the 25 μm stream is about 94%. Comparable results have been obtained from data taken from the other parallel channels.

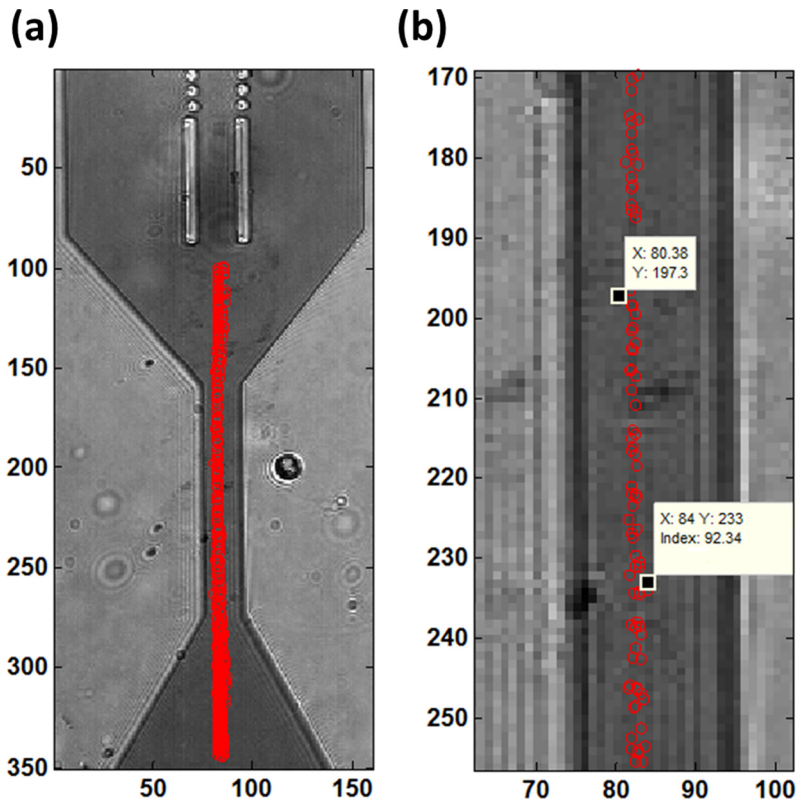

FIG. 10. (a) and (b) M60 cells focused at the detection region for the device with r = 6. The red dots refer to the cells' centroids positions. Cell results stay confined in a range of ≈4 pixels, corresponding to 10 μm, against a channel with a width of 50 μm. The focused stream is not placed at the centre of the channel, but it is slightly shifted on the left due to an asymmetry in the CAD design of the mask used for the fabrication process.

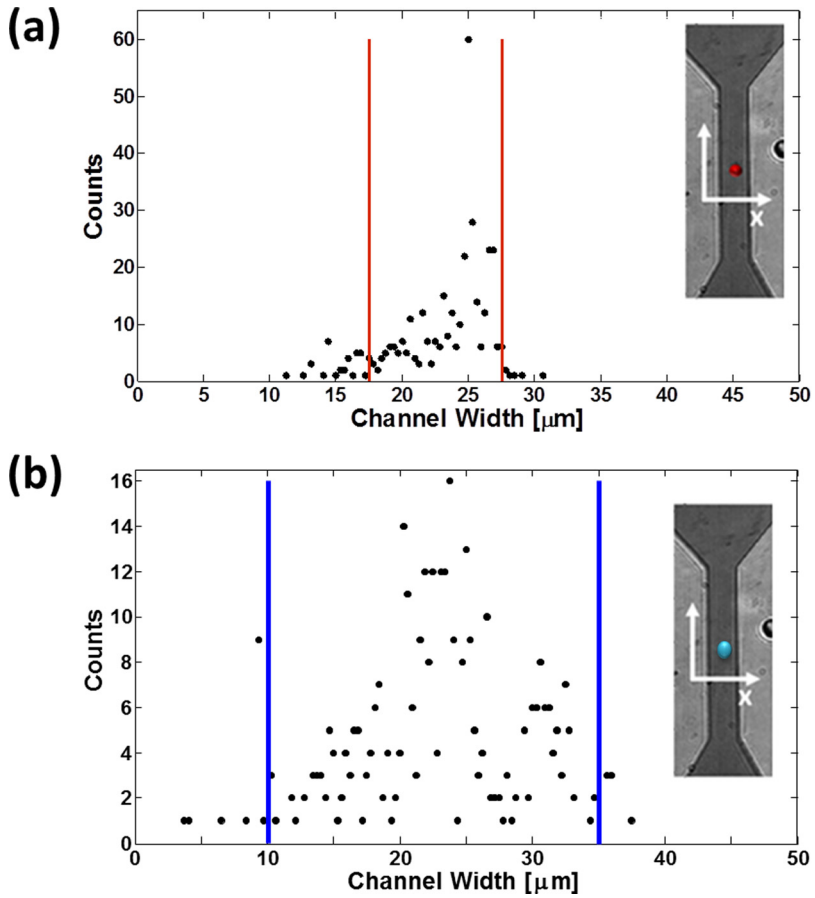

FIG. 11. Distribution of the cell positions across the channel for the high (a) and medium (b) devices. The percentage of total cells that follow within the 10 μm focused region is ≈90% for the device with a high sheath to sample ratio, whilst it is ≈57% for the medium one. For the second device, the percentage of cells confined in a focused stream of 25 μm increases to 94%, as expected from the design analysis.

From the results analysis, it can be concluded that the device with a sheath to sample ratio $r = 6$ is the one that is more suitable for focusing cells with a mean diameter of 10 μm. We obtained results that are highly satisfying since for this device 90% of the cells (94% for the device with $r = 2.5$) stay confined in the focused stream; there are still a 10% of them (6% for the device with $r = 2.5$) that stay out of the focused stream region. From the data analysis, we got that the remaining cells are distributed in an area of ± 5 μm outside the focalized stream. However, these cells have been found in the last acquired videos. The reason for this behaviour is the clogging of some pores in the filter membrane during the operational time. As has been discussed in Sec. III A, the final chip configuration has been optimized in order to allow a device operation of at least 1 h. Getting close to this working time, some pores start to get clogged and the quantity of fluid that moves into the lateral channels decreases. Consequently, Q_{sh} reduces and therefore also $r = Q_{sh}/Q_{sa}$. This brings a widening of the focused stream. This confirms our design assumption that after about 1 h, the filter membrane starts to get clogged. Therefore, in order to increase the operation time in which the focused stream remains tight, slight changes have to be introduced into the geometry of the cross-filter region.

In addition to the previous characterizations, a counting of flowing particles into the realized device has been performed. A green laser was used as the light source. By using a cylindrical lens, a sheet of light was focused on the detection area (Fig. 12). In this way, signals from multiple channels could be simultaneously acquired by using an array of detectors. In our

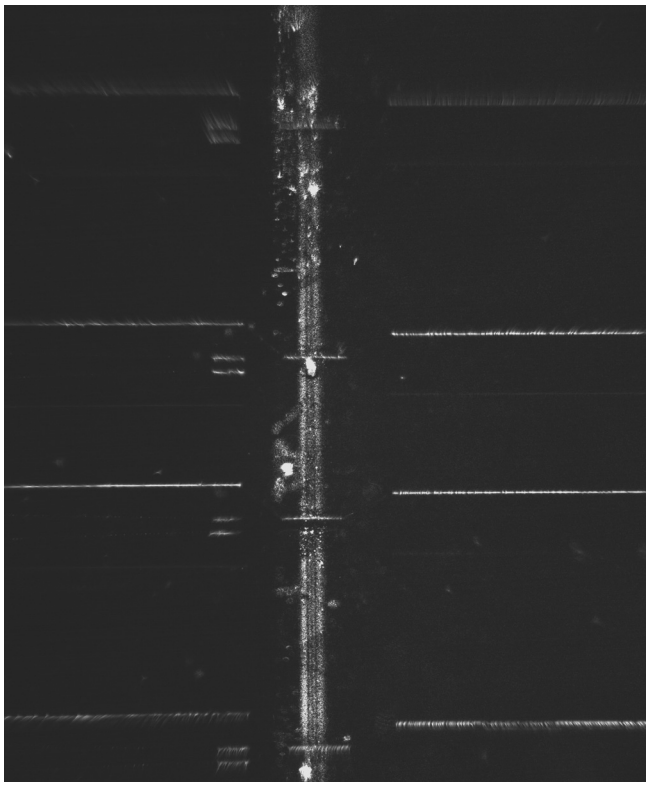

FIG. 12. A particle counting experiment was performed. A green laser was used as an illumination source, and by means of a cylindrical lens, a sheet of light was generated for illuminating all the parallel channels. By using an array of detectors, signals from multiple channels could not be collected at the same time.

experiment, the scattered light was collected using a single PMT (Hamamatsu H6780–01), and the output of the PMT was sent and visualized on an oscilloscope. The flow rate during the experiment was set to 100 μl/min. An average value of 90 particles was counted in a time window of 2 s (Fig. 13). The presence of the eight parallel channels brings an expected total throughput of about 360 cells/s. By setting different values of the experimental parameters, such as acquisition frame rate, flow rate, and particle concentration, different values of the throughput can be achieved.

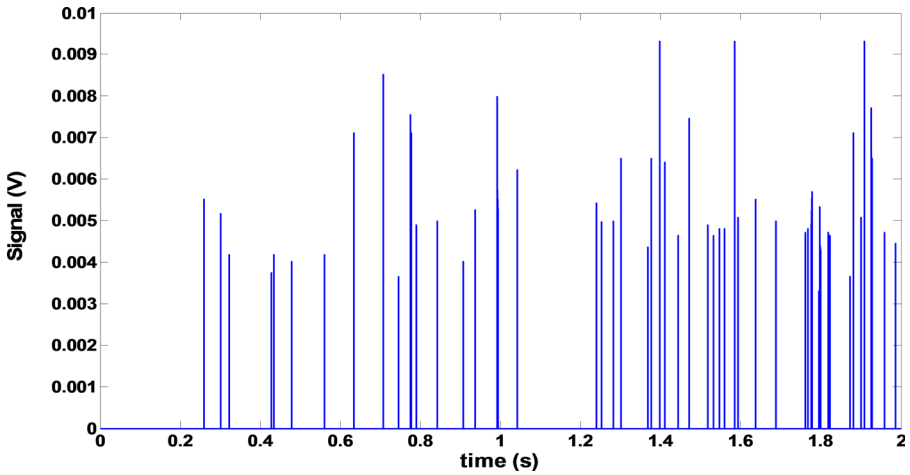

FIG. 13. A 2 s region of the scattered signal collected for a flow-rate of 100 μl/min. Each peak refers to a single 7.5 μm particle passing through the detection region.

V. CONCLUSIONS

Hydrodynamic focusing is the most used method for inducing cell alignment in microfluidic applications. The main drawback in the conventional adopted microfluidic configurations is that multiple inlets are required.

In this work, we have presented a configuration that employing a cross-filter approach allows generating a hydrodynamic focusing without the need for additional inlets for the sheath fluid. This simplification in the geometry leads to the possibility to design a structure with multiple parallel micro-channels, without the need for complicated geometries.

In the hydrodynamic focusing approach, the diameter d of the focused sample stream depends upon the sheath-to-sample flow ratio. By numerical simulation, we have found out the optimal geometry (W_L, L_f, φ) suitable for each particular application. In particular, we realized a cross-filter configuration that allows us to hydro-dynamically focus Acute Lymphoid Leukemia cells from the M60 cell line. The size of these target cells is in the range of 5–8 μm. The performance of the realized device is well-suited to the requirements needed for an imaging flow cytometry approach.

The multiple parallel channels allow reducing the fluid flow velocity during the experiment, by maintaining at the same time a good throughput. In this way, cells can be imaged while they are flowing, avoiding blurring effects, without the need for using highly performing imaging systems. Our results confirm that the proposed approach, taking advantage of the microfluidic technology, is easily integrable into a parallelized device. Therefore, the proposed method could provide useful support in cancer cell analysis thus enabling the realization of an integrated lab-on-chip that allows one to perform both imaging and cytometric analysis. Moreover, this approach well fits the needs of an emerging market interest in realizing lab-on-chip devices that are cheap, disposable, easily transportable and, furthermore, suitable for only one single application,[62–64] conversely to bulky traditional bench-top instrumentations.

ACKNOWLEDGMENTS

This work was supported in part by the FIRB project: Portable pyro-electro-hydrodynamic biosensor as Nano-Bio-Guard for home-land and food security (RBFR10FKZH) from the Ministry of Education, University and Research of Italy, and by Ste.Bi. S.Te.Bi.srl—Biomedical Technologies Society.

[1]F. B. Myersa and L. P. Lee, Lab Chip **8**, 2015 (2008).
[2]S. K. Sia and L. J. Kricka, Lab Chip **8**, 1982 (2008).
[3]C. Sakamoto, N. Yamaguchi, M. Yamada, H. Nagase, M. Seki, and M. Nasu, J. Microbiol. Methods **68**, 643 (2007).
[4]P. R. Chiarot, P. Sullivan, and R. Ben Mrad, J. Microlectromech. Syst. **20**, 1241 (2011).
[5]E. K. Sackmann, A. L. Fulton, and D. J. Beebe, Nature **507**, 181 (2014).
[6]J. Godin, C. H. Chen, S. H. Cho, W. Qiao, F. Tsai, and Y. H. Lo, J. Biophotonics **1**, 355 (2008).
[7]D. Mark, S. Haeberle, G. Roth, F. Von Stetten, and R. Zengerle, Chem. Soc. Rev. **39**, 1153 (2010).
[8]J. J. Shi, S. Yazdi, S. C. S. Lin, X. Y. Ding, I. K. Chiang, K. Sharp, and T. J. Huang, Lab Chip **11**, 2319 (2011).
[9]A. Lenshof, C. Magnusson, and T. Laurell, Lab Chip **12**, 1210 (2012).
[10]M. E. Piyasena, P. P. A. Suthanthiraraj, R. W. Applegate, A. M. Goumas, T. A. Woods, G. P. Lopez, and S. W. Graves, Anal. Chem. **84**, 1831 (2012).
[11]Y. Zhao, B. S. Fujimoto, G. D. Jeffries, P. G. Schiro, and D. T. Chiu, Opt. Express **15**, 6167 (2007).
[12]M. P. MacDonald, G. C. Spalding, and K. Dholakia, Nature **426**, 421 (2003).
[13]T. T. Zhu, R. Cheng, and L. D. Mao, Microfluid. Nanofluid. **11**, 695 (2011).
[14]S. A. Peyman, A. Iles, and N. Pamme, Lab Chip **9**, 3110 (2009).
[15]I. F. Cheng, H. C. Chang, and D. Hou, Biomicrofluidics **1**, 021503 (2007).
[16]S. Park, Y. Zhang, T.-H. Wang, and S. Yang, Lab Chip **11**, 2893 (2011).
[17]J. G. Santiago, Anal. Chem. **73**, 2353 (2001).
[18]L. Wang, L. A. Flanagan, N. Li Jeon, E. Monuki, and A. P. Lee, Lab Chip **7**, 1114 (2007).
[19]J. Gao, R. Riahi, M. L. Y. Sin, S. Zhang, and P. K. Wong, Analyst **137**, 5215 (2012).
[20]S. Choi and J. K. Park, Anal. Chem. **80**, 3035 (2008).
[21]C. Simonnet and A. Groisman, Anal. Chem. **78**, 5653 (2006).
[22]N. Watkins, B. M. Venkatesan, M. Toner, W. Rodriguez, and R. Bashir, Lab Chip **9**, 3177 (2009).
[23]X. Mao, J. R. Waldeisena, and T. J. Huang, Lab Chip **7**, 1260 (2007).
[24]D. R. Gossett and D. Di Carlo, Anal. Chem. **81**, 8459 (2009).
[25]D. Di arlo, D. Irimia, R. G. Tompkins, and M. Toner, Proc. Natl. Acad. Sci. U. S. A. **104**, 18892 (2007).
[26]A. Russom, A. K. Gupta, S. Nagrath, D. Di Carlo, J. F. Edd, and M. Toner, New J. Phys. **11**, 075025 (2009).

[27]X. Xuan, J. Zhu, and C. Church, Microfluid. Nanofluid. **9**, 1 (2010).
[28]R. Scott, P. Sethu, and C. K. Harnett, Rev. Sci. Instrum. **79**, 046104 (2008).
[29]X. Mao, A. A. Nawaz, S.-C. S. Lin, M. I. Lapsley, Y. Zhao, J. P. McCoy, W. S. El-Deiry, and T. J. Huang, Biomicrofluidics **6**, 024113 (2012).
[30]A. A. Nawaz, X. Zhang, X. Mao, J. Rufo, S. S. Lin, F. Guo, Y. Zhao, M. Lapsley, P. Li, J. P. McCoy, S. J. Levine, and T. J. Huang, Lab Chip **14**, 415 (2014).
[31]S. Choi, S. Song, C. Choi, and J. K. Park, Small **4**, 634 (2008).
[32]S. Choi, S. Song, C. Choi, and J. K. Park, Anal. Chem. **81**, 50 (2008).
[33]X. Wang, M. Zandi, C. C. Ho, N. Kaval, and I. Papautsky, Lab Chip **15**, 1812 (2015).
[34]A. J. Chung, D. R. Gossett, and D. Di Carlo, Small **9**, 685 (2013).
[35]D. Di Carlo, Lab Chip **9**, 3038 (2009).
[36]S. C. Hur, H. T. K. Tse, and D. Di Carlo, Lab Chip **10**, 274 (2010).
[37]A. Karimi, S. Yazdi, and A. M. Ardekani, Biomicrofluidics **7**, 021501 (2013).
[38]J. Y. Kim, S. W. Ahn, S. S. Lee, and J. M. Kim, Lab Chip **12**, 2807 (2012).
[39]J. M. Martel and M. Toner, Sci. Rep. **3**, 3340 (2013).
[40]D. A. Basiji, W. E. Ortyn, L. Liang, V. Venkatachalam, and P. Morrissey, Clin. Lab Med. **27**, 653 (2007).
[41]A. E. Dawson, J. A. Norton, and D. S. Weinberg, Am. J. Pathol. **136**, 1115 (1990).
[42]B. K. McKenna, H. Salim, F. R. Bringhurst, and D. J. Ehrlich, Lab Chip **9**, 305 (2009).
[43]E. Schonbrun, A. R. Abate, P. E. Steinvurzel, D. A. Weitz, and K. B. Crozier, Lab Chip **10**, 852 (2010).
[44]B. K. McKenna, J. G. Evans, M. C. Cheung, and D. J. Ehrlich, Nat. Methods **8**, 401 (2011).
[45]E. Schonbrun, S. S. Gorthi, and D. Schaak, Lab Chip **12**, 268 (2012).
[46]M. V. VanDelinder and A. Groisman, Anal. Chem. **78**, 3765 (2006).
[47]H. Mohamed, J. N. Turner, and M. Caggana, J. Chromatogr. A **1162**, 187 (2007).
[48]D. F. Chen, C. C. Cui, and H. L. Liu, Sens. Actuators, B **130**, 216 (2008).
[49]B. Keskinler, E. Yildiz, E. Erhan, M. Dogru, Y. K. Bayhan, and G. Akay, J. Membr. Sci. **233**, 59 (2004).
[50]S. C. Gifford, A. M. Spillane, S. M. Vignes, and S. S. Shevkoplyas, Lab Chip **14**, 4496 (2014).
[51]P. Bacchin, Q. Derekx, D. Veyret, K. Glucina, and P. Moulin, Microfluid. Nanofluid. **17**, 85 (2014).
[52]G. Foley, J. Membr. Sci. **274**, 38 (2006).
[53]M. Yamada and M. Seki, Anal. Chem. **78**, 1357 (2006).
[54]R. Aoki, M. Yamada, M. Yasuda, and M. Seki, Microfluid. Nanofluid. **6**, 571 (2009).
[55]L. R. Huang, E. C. Cox, R. H. Austin, and J. C. Sturm, Science **304**, 987 (2004).
[56]K. J. Morton, K. Loutherback, D. W. Iglis, O. K. Tsui, J. C. Sturm, S. Y. Chou, and R. H. Austin, Proc. Natl. Acad. Sci. **105**, 7434 (2008).
[57]S. H. Faderl, H. M. Kantarjian, and E. H. Estey, *Hematologic Malignancies: Acute Leukemias* (Springer, Berlin, Heidelberg, 2008).
[58]C. Cobaleda and I. Sánchez-García, Bioessays **31**, 600 (2009).
[59]H. Bruus, *Theoretical Microfluidics* (Oxford University Press, Oxford, 2008).
[60]R. J. Adrian, Exp. Fluids **39**, 159 (2005).
[61]J. G. Santiago, C. D. Meinhart, S. T. Wereley, D. J. Beebe, and R. J. Adrian, Express Fluids **25**, 316 (1998).
[62]J. H. Wang, C. H. Wang, C. C. Lin, H. Y. Lei, and G. B. Lee, Microfluid. Nanofluid. **10**, 531 (2011).
[63]U. Hassan and R. Bashir, Lab Chip **14**, 4370 (2014).
[64]Q. Guo, S. P. Duffy, K. Matthews, A. T. Santoso, M. D. Scott, and H. Ma, J. Biomech. **47**, 1767 (2014).
[65]See supplementary material at http://dx.doi.org/10.1063/1.4936260 for a movie showing the effect of the self-induced hydrodynamic focusing on cells for the strong focusing device (movie 1).